Journal of Catalysis **204,** 169–174 (2001)
doi:10.1006/jcat.2001.3373, available online at http://www.idealibrary.com on IDEAL®

# The Structure of Carbon Encapsulated NiFe Nanoparticles

Wendy Teunissen,* Frank M. F. de Groot,*,[1] John Geus,* Odile Stephan,† Marcel Tence,† and Christian Colliex†,‡

*Debye Institute, Department of Inorganic Chemistry and Catalysis, Utrecht University, Sorbonnelaan 16, 3584 CA, Utrecht, The Netherlands; †Laboratoire de Physique des Solides, Bâtiment 510, CNRS UMR 8502, F 91405 Orsay, France; and ‡Laboratoire Aimé Cotton, Bâtiment 505, CNRS UPR 3321, F 91405 Orsay, France

Received April 26, 2001; revised June 26, 2001; accepted August 4, 2001

**Carbon encapsulated NiFe nanoparticles (NiFe@C) have been prepared by high-temperature methane encapsulation of the bare bimetallic particles on alumina. High-resolution transmission electron microscopy pictures show that about 6-nm thick carbon layers encapsulate 10–20-nm diameter NiFe nanoparticles. The NiFe nanoparticles are shown to be single-crystalline and no carbide is found at the NiFe–C interface. This is confirmed by the electron energy-loss spectroscopy (EELS) measurements that in addition show that both Ni and Fe have a zero (metal) valence and that only graphite is present. EELS also shows that the nickel-to-iron ratio is exactly unity for all particles studied. Metallic Pd nanoparticles with a diameter of 1–2 nm can be anchored on the carbon layers, which creates a Pd/NiFe@C type of catalyst that could be used for liquid phase reactions. The EELS analysis reveals that part of the nanoparticles present are not Pd but other oxidic carbon encapsulated nanoparticles.** 

*Key Words:* **carbon encapsulation; TEM; EELS; magnetic separation.**

## INTRODUCTION

A major goal in catalysis research is the development of small solid bodies that can be suspended in and extracted from the liquid phase. These bodies need to be small to overcome the transport limitations in the liquid phase. Bodies smaller than a few $\mu$m cannot be separated by filtration or centrifugation. Magnetic separation offers a route to use particles of about 50 nm, but requires these nanoparticles to have a sufficiently high saturation magnetization, while redispersion asks for magnetic softness. NiFe and CoFe bimetallic systems are satisfactory candidates from the magnetic point of view. For the particles to be used as catalytic support material, they must be inert and resistant to the conditions during catalytic reactions. Bare metallic nanoparticles certainly do not fulfill these requirements and a solution is the embedding of the bimetallic nanoparticles in carbon sheets.

Carbon encapsulation has attracted much attention after the discoveries of fullerenes, single-walled carbon tubes, and related systems (1, 2). Multiwalled carbon fibers, also known as carbon filaments, have a long history, ever since the 1889 patent on the growth of carbon filaments by metal crucibles (3). Throughout the twentieth century the nucleation and growth of carbon fibers has been an important field of research, mainly because of the destructive nature of carbon fibers on reactor walls (4, 5). The knowledge of the prevention of carbon fiber growth automatically yielded new insights on the optimization of carbon fiber growth modes and, closely related, on the growth of encapsulated metal particles (5).

## EXPERIMENTAL

Carbon encapsulated NiFe particles (NiFe@C) have been prepared by (a) growing NiFe metal particles on $\gamma$-alumina, (b) encapsulating these NiFe metal particles in a methane flow, followed by removal of alumina and also any incompletely covered particles with an acid treatment, and (c) having Pd nanoparticles anchored on the outside of the carbon encapsulated particles. Compared to the arc discharge method (1, 6–9), as well as other methods (10–12), this catalytic route to the production of carbon encapsulated nanoparticles offers a much more detailed control of, for example, the alloy composition. In addition, scaleup is expected to be easier.

(a) The NiFe particles are prepared by depositing *sodium nitroferricyanide* ($Na_2Fe(CN)_5NO$) and *nickel nitrate* $Ni(NO_3)_2$ precursors, which have a nickel-to-iron ratio of 1 : 1. The aqueous iron cyanide solution is injected at a rate of 1 ml/min into a vigorously stirred suspension of $\gamma$-alumina in an aqueous solution of nickel nitrate and kept at pH 5. The NiFe loaded alumina was filtered, washed, and dried at room temperature in a vacuum for 24 h. The 425–850-$\mu$m sieve fraction was calcined in a 95 ml/min flow of 20% oxygen in helium at 573 K for 3 h. This gives NiFe–oxide particles on alumina. This treatment is followed by a reduction in a 100 ml/min flow of 20% hydrogen in argon

[1] To whom correspondence should be addressed. Fax: ++31 30 2511027. E-mail: f.m.f.degroot@chem.uu.nl.



0021-9517/01 $35.00

at 700°C for 2 h. This gives about 20 wt% bare NiFe alloy particles on $\gamma$-alumina (13, 14).

(b) The encapsulation procedure is based on the large body of knowledge developed for the growth of carbon fibers (5). The alloy particles were brought to 998 K under flowing hydrogen, exposed to a 100 ml/min flow of 20% methane in argon at 998 K for 1 h and cooled to room temperature in a flow of argon. This yields carbon encapsulated NiFe particles as well as partly uncovered alloy particles. To isolate the encapsulated NiFe particles, 200 mg of alumina was dissolved by boiling the sample with 50-ml concentrated hydrochloric acid for 30 min. 200 ml of cold demineralized water was added and the material was filtered, washed, and dried in air at room temperature. The acid treatment has removed all NiFe particles with porous carbon layers, in this way excluding the presence of nickel–iron alloy particles in not fully closed shells. The relative yield of the NiFe particles prepared in this manner is 68% (14).

(c) To prepare NiFe@C supported palladium catalysts, we used incipient wetness impregnation with $PdCl_2$ dissolved in hydrochloric acid. It turned out from previous research on carbon fibers that no further activation procedure is required for anchoring the palladium complex on the carbon (15, 16). The pore volume (voids between the spherical NiFe@C particles) of the material was measured to be 0.9 ml/g. To prepare a catalyst with a Pd loading of 2.5 wt%, NiFe@C was placed in an impregnation flask and brought under static vacuum. The calculated amount of the Pd solution was injected into the flask and kept under static vacuum for 15 min. Next, an argon flow was passed over at a temperature of 333 K for 1 h. The Pd complex anchored to the carbon layers was converted to metallic palladium upon reduction in hydrogen. Samples of Pd/NiFe@C were placed in a reactor in a gas flow of 10% $H_2$ in Ar, raising the temperature with 1.5 K/min to 473 K.

## RESULTS AND DISCUSSION

The geometric and electronic structure of NiFe@C particles has been characterized with transmission electron microscopy (TEM) and electron energy-loss spectroscopy (EELS) using a scanning TEM. The TEM images were acquired with a Topcon 002B electron microscope operating at 200 kV, equipped with a $LaB_6$ filament, and providing a point resolution of about 0.2 nm. Samples were prepared by suspending the solid in ethanol under ultrasonic vibration. One or two drops of the thus prepared suspension were brought onto a punched carbon film on a copper grid. The EELS data were recorded with a scanning transmission electron microscope VG HB 501, equipped with a field-emission source and a parallel Gatan 666 EELS spectrometer. This instrument produces EELS spectra with a typical 0.7-eV resolution recorded from subnanometer areas

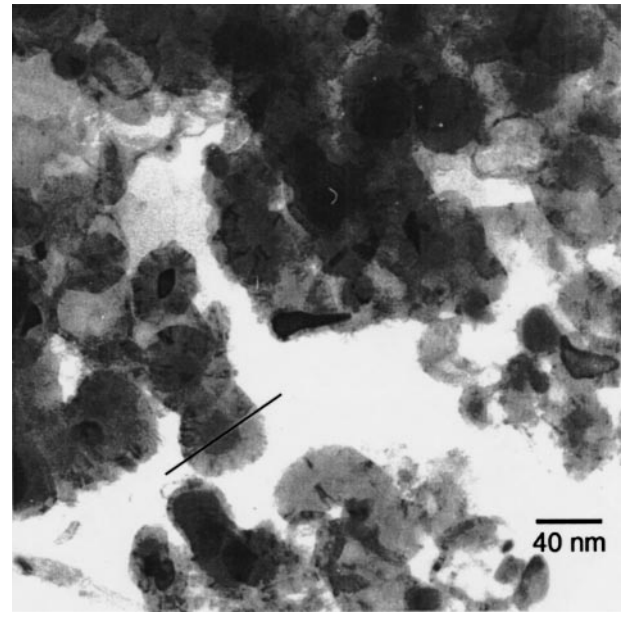


**FIG. 1.** TEM image of carbon coated nickel–iron particles. The line indicates the probe position during the EELS analyses.

(17, 18). In the line-spectrum mode, spectra are recorded while ramping the probe with given steps across the specimen. Acquisition times required for achieving a satisfactory signal-to-noise level on core edges are on the order of 100 ms–1 s. A checking of the materials after EELS measurements indicated that there was no radiation-induced structural damage.

A TEM picture of the particles is shown in Fig. 1. The metallic core is encapsulated in polyhedral concentric graphitic shells with a varying number of layers. Figure 2 shows a high-resolution photo of the lattices of the metallic core and the surrounding carbon. From this figure the lattice distance found for the NiFe core is 0.21 nm, in agreement with the (111) lattice dimension of metallic NiFe. For graphite we measured a lattice distance of 0.34 nm, close to its (002) lattice. All particles studied showed only one orientation of the NiFe lattice, without grain boundaries. This indicates that the particles measured are single crystals. As far as detectable from the images, no dissimilarity in the lattice distances are observed at the interface of the NiFe metal core and the carbon layers. This indicates that no carbidic phase is present, an observation that will be confirmed by the EELS measurements.

An EELS spectrum, taken at a probe position on the NiFe metal core is represented in Fig. 3. The electron, energy-loss fine structure of the carbon K edge at 280 eV, the iron $L_{2,3}$ edge at 710 eV, and nickel $L_{2,3}$ edge at 850 eV are clearly visible. The iron and nickel edges are much weaker than the carbon K edge and they have been multiplied by 8.0 in Fig. 3. The spectral shapes of the EELS core edges provide chemical information on the nature of the elements

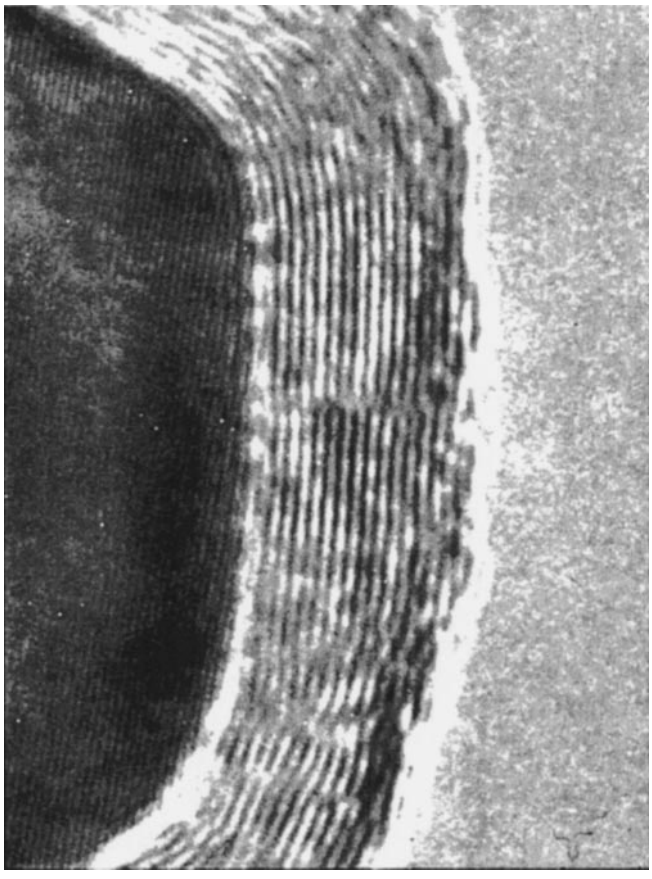

**FIG. 2.** High-resolution TEM image of the NiFe core and the surrounding graphite layers. The graphite layer thickness is approximately 6 nm.

(19, 20). The nickel and iron $L_{2,3}$ spectra (shown with better statistics in Fig. 5) indicate metallic nickel respectively iron (21), while the carbon K edge is reminiscent of graphitic carbon.

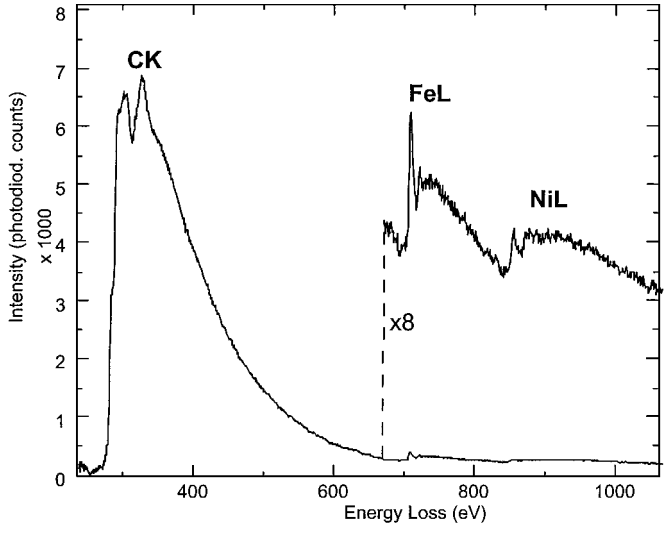


**FIG. 3.** Electron energy loss fine structure of the carbon K edge and the iron and nickel L edge. The spectrum is taken at one probe position.

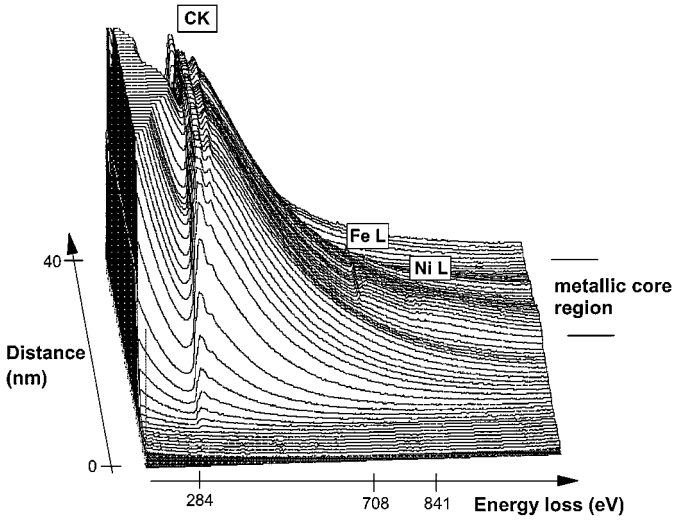


**FIG. 4.** 2D plot of a line spectrum (64 spectra) as the probe beam scans along a line of approximately 40 nm from vacuum through a 35-nm NiFe@C particle. Horizontal scans represent the energy-loss values.

Figure 4 represents the 2D plot of a sequence of spectra taken across a particle of about 35 nm with a metallic core of about 12 nm. The path was chosen through the center of the particle as indicated in Fig. 1. The sequence of 64 spectra was recorded with a 0.5-nm probe, a 0.6-nm pixel increment, and an acquisition time of 1 s per pixel. This amounts to a total path length of 40 nm within a total acquisition time of 64 s. To obtain the nickel-to-iron ratio within the alloy particle, the cross sections of the carbon K edge, nickel L edge, and iron L edge were estimated for every EELS spectrum. Figure 5 shows part of one EELS spectrum. The region used for background subtraction is indicated before the iron and nickel edges and the resulting background is given as the

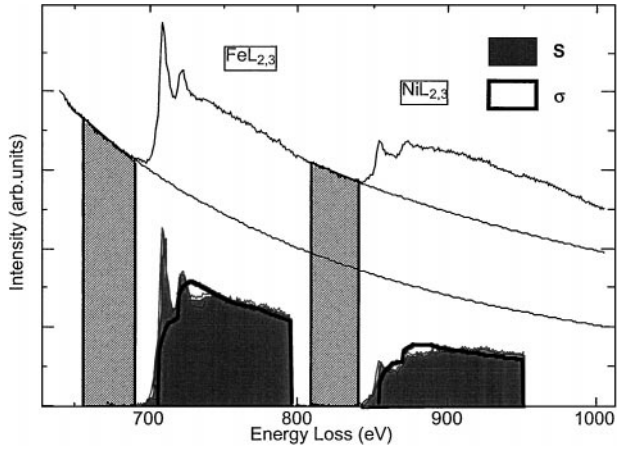


**FIG. 5.** $L_{2,3}$ edges for iron and nickel recorded from carbon encapsulated particles. Also shown are the two characteristic signals after background subtraction, the energy window for integration of the characteristic signals and calculated ionization cross sections, and the calculated atomic cross sections calculated in a Hartree–Slater model.

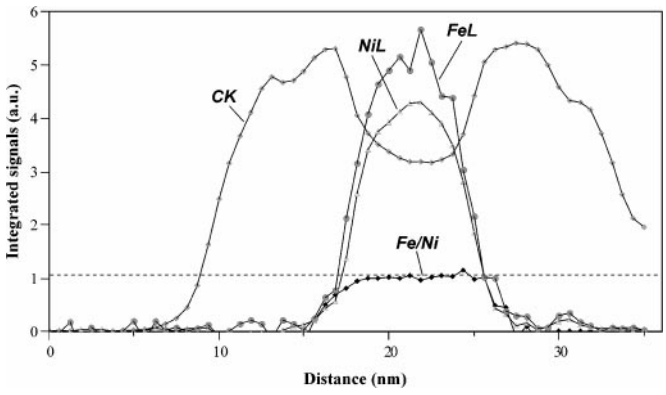


**FIG. 6.** The normalized intensity variations of the carbon K, nickel $L_{2,3}$, and iron $L_{2,3}$ edges as the beam is scanned across an encapsulated NiFe particle.

thin lines. The characteristic signals after background subtraction are shown with filled surfaces, indicating also the energy window for integration of the characteristic signals and the calculated ionization cross sections (22). In order to improve the statistics and limit potential sample damage, we did measure the EELS spectra over the core level region only; i.e., the plasmon region was not detected in parallel. We note that this has the disadvantage that for thick samples it is not possible to correct the intensity profile for multiple scattering events.

The results of the analysis have been summarized in Fig. 6. No elements other than carbon, nickel, and iron were detected. As the beam scans across the particle, the intensity of the energy-loss peaks corresponding with the K edge in graphite (window: 280–325 eV) increases corresponding with the increasing number of carbon atoms in the column that the beam encounters, exhibits a drop in the center due to the internal hollow space, and follows the same pattern on the other side. The shape of the profile essentially shows a cylindrical geometry (23), which is in agreement with a small slice in the center of a spherical particle projected in a two-dimensional way. A distortion from a perfect hollow sphere can be observed in the small dip around the position at 14 nm. This indicates that the graphitic layer deviates from a perfect sphere. The intensity of the energy loss from the $L_{2,3}$ edges of nickel and iron correlates well with the position of the central core of the particle and the peaking of intensity in the center clearly indicates that the alloyed nickel and iron is present as a solid sphere and is not just wetting the inside surface. An elemental quantification using tabulated atomic 2p ionization cross sections (24) gives a constant ratio of nickel and iron very close to unity, in agreement with the adjusted nickel-to-iron ratio in the cyanide complex used during preparation, namely $NiFe(CN)_5NO$. A similar result was found for all six investigated particles. In summary, the shape of the different curves in Fig. 6 confirms the approximately spherical geometry of the particle, with a hollow core for carbon, filled with a solid core with a nickel-to-iron ratio of unity.

No spectral variations were found across the iron and nickel $L_{2,3}$ edges in the particle core and also at the interface with graphite. The iron and nickel spectral shapes (cf. Fig. 5) indicate that both are present in their metallic state (21). The carbon K edge indicated in Fig. 3 corresponds to graphite and shows no indication for the presence of any carbidic species in the filled portion of the particle. The high-temperature synthesis of the surrounding graphite layers seems to result in nonsegregated, NiFe alloy particles encapsulated by closed shells of pure graphite with the absence of carbides at the interface. However, the comment must be made that a carbidic phase formed during synthesis, not finally resulting in nonporous surrounding graphitic layers, will be removed during treatment in hydrochloric acid. This result confirms the HRTEM images (cf. Fig. 2), where also no indication was found for a carbidic phase.

### *Anchoring of Pd Particles*

A TEM micrograph of a NiFe@C-supported palladium catalyst after reduction is represented in Fig. 7. Clearly visible are the small particles on the external edge of the carbon layers. Most of these particles turned out to be metallic Pd, but as will be discussed below other types of small particles were found from the EELS analysis. The large particles are the ferromagnetic NiFe cores of the support. Apart from small particles on the outside of the NiFe@C particles, also small particles are visible at other positions in the sample,

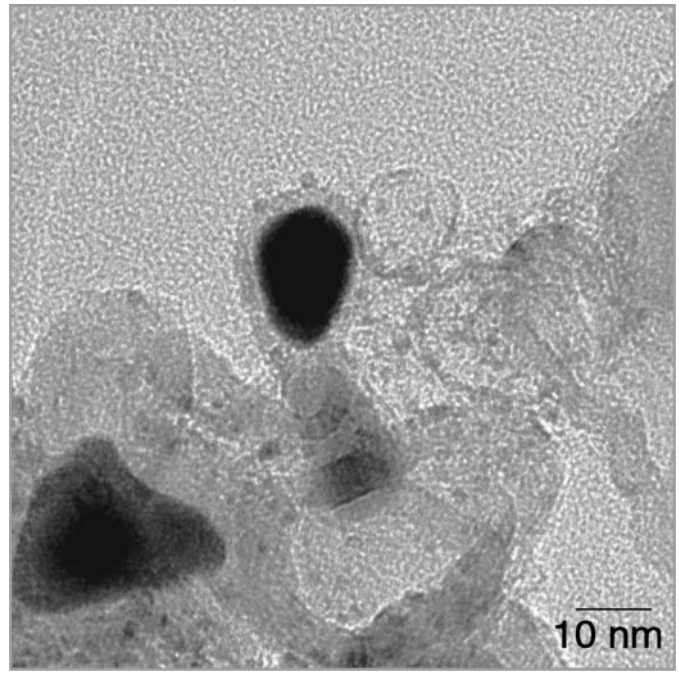


**FIG. 7.** TEM images of palladium on NiFe@C, prepared via impregnation.

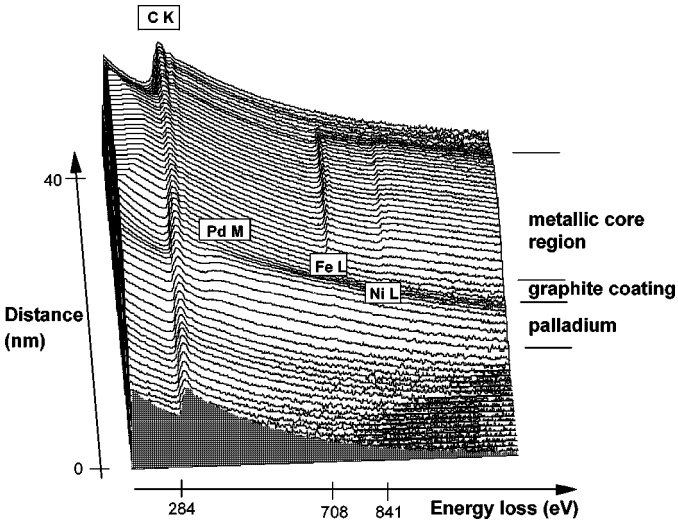


**FIG. 8.** 2D plot of a line spectrum along a line of approximately 40 nm from vacuum through a 60-nm Pd/NiFe@C particle. Horizontal scans represent the energy-loss values.

for example, on the empty sphere to the right of the NiFe@C particle.

Figure 8 shows the 2D plot of a sequence of spectra taken halfway across a particle of about 60 nm with a metallic core of about 40 nm. The sequence was recorded in the same manner as Fig. 4. In addition to the carbon K edge at 280 eV, the iron $L_{2,3}$ edge at 710 eV, and the nickel $L_{2,3}$ edge at 850 eV, the Pd $M_{2,3}$ edge at 532 eV can be observed. Figure 9 displays the profile of the relative intensities of Pd, C, Ni, and Fe calculated from the line scan shown in Fig. 8 and using the same procedure as described above for the NiFe@C particles. The carbon profile of Fig. 9 agrees with an almost perfect hollow spherical carbon particle. Palladium is located on the external edge of the particle, anchored to the carbon layers. A particle with a diameter of approximately 5 nm is found in Fig. 9. The spectral shape of the Pd $M_{2,3}$ edge shows that Pd is in its metallic state. However, we should mention that the detection of a small amount of oxygen is complicated due to the presence of the Pd $M_3$ edge in the O K energy range. We were not able to detect any deviation of the Pd or C spectra at the Pd/C interface, but we cannot rule out detection limitations due to the very small interface area. The iron-to-nickel ratio is constant throughout the particle, but deviates from the adjusted 1 : 1 ratio.

All particles with a NiFe core less than 12 nm in diameter show exactly the 1 : 1 ratio. Therefore we believe that this deviation is due to the incorrect background modeling and the consequent incorrect evaluation of the characteristic absorption signals. As indicated above, we did not measure the plasmon region of the EELS spectrum simultaneously, which excludes the elimination of multiple scattering effects. The Ni : Fe ratio in Fig. 9 is still found to be constant over the core of particle. This ratio seems to increase in the carbon region between the NiFe core and palladium nanoparticle. However, as the absolute Ni and Fe intensities decrease in this region, the uncertainty in the ratio increases and the determined value is not reliable enough to draw a firm conclusion.

A systematic scan on all small particles that are observable with EELS in a certain area showed that only about half of these particles consisted of Pd. Some of the small particles we examined turned out to be iron oxide or nickel–iron oxide, fully covered with graphite, where in some cases also aluminium is present. In Fig. 10 the EELS spectrum is shown of the analysis of a nickel–iron oxide particle, obtained by using the gain variation routine in the derivative mode. The particles found can originate from the interlayer between the metal and alumina support, which often is hard to reduce. With the formation of encapsulating graphite

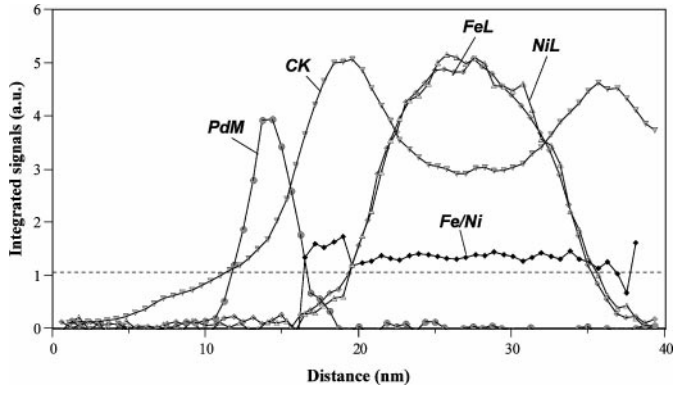


**FIG. 9.** The variation of intensity of carbon K, palladium $M_{2,3}$, nickel $L_{2,3}$, and iron $L_{2,3}$ edges as the beam is scanned across a Pd/NiFe@C particle.

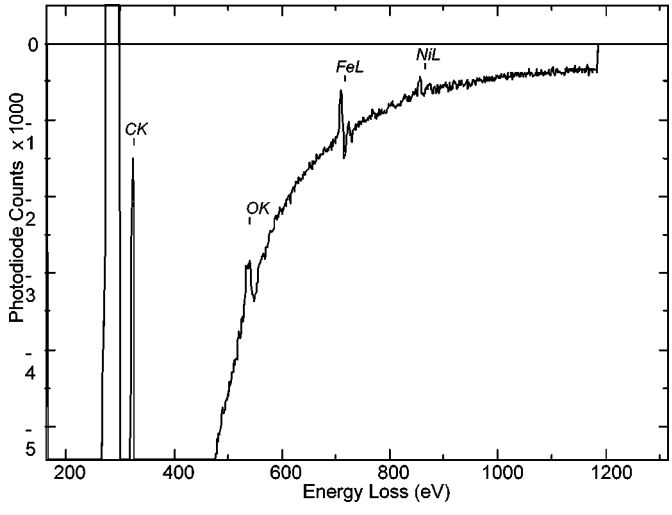


**FIG. 10.** Electron energy-loss fine structure of the carbon K edge, the oxygen K edge, and the iron and nickel $L_{2,3}$ edge. The spectrum is obtained using the gain variation routine, recorded in the derivative mode.

layers the interaction between the alloy particles and support has to be overcome. We suggest that the interface be broken up, leaving some particles in the oxidic phase which become fully encapsulated. These iron oxide, or nickel–iron oxide, encapsulated particles will also be present in the sample where no palladium is anchored to the NiFe@C particles. However, in a TEM picture a palladium nanoparticle of 2 nm will be better visible than a 2-nm NiFe–oxide particle. It is only with an EELS analysis that these nanoparticles reveal their elemental nature.

## CONCLUSIONS

It can be concluded that TEM–EELS provides a detailed picture of the nature of the carbon encapsulated metal particles. The EELS intensity profiles reveal the relative ratio of the elements present. It should be noted that EELS intensity profiles have a spatial resolution of approximately 0.5 nm, which is intrinsically much better than the resolution that can be obtained from an EDX elemental analysis. The EELS elemental analysis is quantitatively correct for thin samples. For samples with a thickness larger than about 30 nm, EELS can also yield quantitatively correct values if the values are corrected for multiple scattering events. The high spatial resolution of the EELS spectra has been used to study potential chemical interface effects. These effects were not observed with the resolution of 0.5 nm.

The NiFe core is found to be metallic and single-crystalline with a lattice distance equal to bulk NiFe and with exactly a 1 : 1 Ni : Fe ratio. The diameter of the particles varies between 10 and 30 nm. The particle is encapsulated by graphitic planes with an interplanar distance equal to bulk graphite. The graphite forms a hollow sphere around the NiFe nanoparticle and no carbidic interface between the metal core and the graphite is visible.

We conclude that the preparation method for anchoring small Pd particles to carbon encapsulated NiFe particles is very effective. This keeps alive promises for the development of encapsulated metal particles as catalyst support materials that can be suspended in, magnetically extracted from, and redispersed in the liquid phase.

Half of the small nanoparticles observed in TEM are related to carbon encapsulated oxides, which is a result that could only be obtained from the EELS analysis. It would be very hard to distinguish such oxidic particles from the Pd particles using TEM only.

## ACKNOWLEDGMENTS

This work was carried out as part of the Innovation Oriented Research Programme on Catalysis (IOP Catalysis IKA94080) sponsored by the Netherlands Ministry of Economic Affairs. The research of FdG has been supported by the Netherlands Research Combination Catalysis.

## REFERENCES

1. Kratschmer, W., Lamb, L. D., Fostiropoulos, K., and Huffman, D. R., *Nature* **347**, 354 (1990).
2. Iijima, S., *Nature* **354**, 56 (1991).
3. Hughes, T. V., and Chambers, C. R., U.S. Patent 405, 480 (1889).
4. Rostrup-Nielsen, J. R., *J. Catal.* **85**, 31 (1984).
5. de Jong, K. P., and Geus, J. W., *Chem. Eng. Rev. Sci. Eng.* **42**, 481 (2000).
6. Dravid, V. P., Host, J. J., Teng, M. H., Elliot, B., Hwang, J., Johnson, D. L., Mason, T. O., and Weertman, J. R., *Nature* **374**, 602 (1995).
7. Scott, J. H. J., and Majetlich, S. A., *Phys. Rev. B* **52**, 12,564 (1995).
8. Dong, X. L., Zhang, Z. D., Jin, S. R., and Kim, B. K., *J. Appl. Phys.* **86**, 6701 (1999).
9. Sun, X., Gutierrez, A., Yacaman, M. J., Dong, X. L., and Jin, S., *Mat. Sci. Eng. A* **286**, 157 (2000).
10. Nolan, P. E., Lynch, D. C., and Cutler, A. H., *J. Phys. Chem. B* **102**, 4165 (1998).
11. Nolan, P. E., Lynch, D. C., and Cutler, A. H., *Carbon* **31**, 817 (1996).
12. Harris, P. J. F., and Tsang, S. C., *Chem. Phys. Lett.* **293**, 53 (1998).
13. Teunissen, W., and Geus, J. W., *Stud. Surf. Sci. Catal.* **121**, 185 (1998).
14. Teunissen, W., Bol, A. A., and Geus, J. W., *Catal. Today* **48**, 329 (1999); Wendy Teunissen, Ph.D. thesis. Utrecht University, Utrecht, The Netherlands, 2000.
15. Hoogenraad, M. S., van Leeuwarden, R. A. G. M. M., van Breda Vriesman, G. J. B., Broersma, A., van Dillen, A. J., and Geus, J. W., *Stud. Surf. Sci. Catal.* **91**, 263 (1995).
16. Mojet, B. L., Hoogenraad, M. S., van Dillen, A. J., Geus, J. W., and Koningsberger, D. C., *J. Chem. Soc. Faraday Trans.* **93**, 4371 (1997).
17. Jeanguillaume, C., and Colliex, C., *Ultramicroscopy* **28**, 252 (1989).
18. Colliex, C., Tencé, M., Lefèvre, E., Mory, C., Gu, H., Bouchet, D., and Jeanguillaume, C., *Mikrochim. Acta* **71**, 114 (1994).
19. Colliex, C., *in* "NATO ASI Series, Series B: Physics" (P. S. Bagus, G. Pacchioni, and F. Parmigiani, Eds.), Vol. 345, p. 213, Colliex, C., *J. Electron. Microsc.* **45**, 44 (1996).
20. de Groot, F. M. F., *J. Elec. Spectrosc.* **67**, 529 (1994).
21. Fink, J., Müller-Heinzerling, Th., Scheerer, B., Speier, W., Hillebrecht, F. U., Fuggle, J. C., Zaanen, J., and Sawatzky, G. A., *Phys. Rev. B* **32**, 4899 (1985).
22. Egerton, R. F., *in* "Electron Energy-Loss Spectroscopy in the Electron Microscope." Plenum, New York, 1986.
23. Suenaga, K., Colliex, C., Demoncy, N., Loiseau, A., Pascard, H., and Williame, F., *Science* **278**, 653 (1997).
24. Leapman, R. D., Rez, P., and Mayers, D. F., *J. Chem. Phys.* **72**, 1232 (1980).